

# Cubic magneto-optic Kerr effect in Ni(111) thin films with and without twinning

Maik Gaerner,<sup>1,\*</sup> Robin Silber,<sup>2,3,\*</sup> Tobias Peters,<sup>1</sup> Jaroslav Hamrle,<sup>4</sup> and Timo Kuschel<sup>1,†</sup>

<sup>1</sup>*Center for Spinelectronic Materials and Devices,*

*Department of Physics, Bielefeld University, Bielefeld 33615, Germany*

<sup>2</sup>*IT4Innovations, VŠB-Technical University of Ostrava, Ostrava 70800, Czech Republic*

<sup>3</sup>*Nanotechnology Centre, VŠB-Technical University of Ostrava, Ostrava 70800, Czech Republic*

<sup>4</sup>*Faculty of Mathematics and Physics, Charles University, Prague 12116, Czech Republic*

In most studies utilizing the magneto-optic Kerr effect (MOKE), the detected change of polarized light upon reflection from a magnetized sample is supposed to be proportional to the magnetization  $\mathbf{M}$ . However, MOKE signatures quadratic in  $\mathbf{M}$  have also been identified and utilized, e.g., to sense the structural order in Heusler compounds, to detect spin-orbit torques or to image antiferromagnetic domains. In our study, we observe a strong anisotropic MOKE contribution of third order in  $\mathbf{M}$  in Ni(111) thin films, attributed to a cubic magneto-optic tensor  $\propto \mathbf{M}^3$ . We further show that the angular dependence of cubic MOKE (CMOKE) is affected by the amount of structural domain twinning in the sample. Our detailed study on CMOKE for two selected photon energies will open up new opportunities for CMOKE applications with sensitivity to twinning properties of thin films, e.g. CMOKE spectroscopy and microscopy or time-resolved CMOKE.

*I. Introduction* - The magneto-optic Kerr effect (MOKE) [1], being magnetic circular dichroism and birefringence upon reflection from a magnetized sample, serves as a powerful tool in the area of thin-film magnetic characterization [2, 3]. So far, applications such as vectorial magnetometry [4, 5], MOKE spectroscopy [6, 7] and microscopy [8, 9] as well as time-resolved MOKE [10, 11] mainly rely on linear MOKE (LinMOKE), being linearly proportional to the magnetization  $\mathbf{M}$ .

In addition, quadratic-in-magnetization MOKE (QMOKE) [12, 13], being magnetic linear dichroism and birefringence upon reflection proportional to  $\mathbf{M}^2$ , can be employed to study antiferromagnets, for example in time-resolved experiments [14–16]. QMOKE showed to be sensitive to the structural ordering of Heusler compounds [17, 18] and to spin-orbit torque effects [19]. Vectorial magnetometry including QMOKE [20–24], QMOKE spectroscopy [18, 25–28], as well as QMOKE microscopy [29, 30] have been realized.

However, any higher-order MOKE, such as cubic-in-magnetization MOKE (CMOKE), being proportional to  $\mathbf{M}^3$ , has only been mentioned very rarely so far [31–33] and has not yet been systematically investigated. Furthermore, higher-order transport effects have been detected in magnetoresistive and anomalous Hall effects [34–36] and can be expected analogously for magneto-thermal and anomalous Nernst effects. Those effects possess equal symmetries as in the case of MOKE. However, MOKE offers advantages for spectroscopy, microscopy and time-resolved experiments that electrical measurements cannot provide such as spectral range, spatial and time resolution.

In this letter, we report on the observation of third-order-in-magnetization MOKE in Ni(111) thin films. We identify this CMOKE as a threefold in-plane angular dependence of the magnetically saturated longitudinal MOKE (LMOKE) response which cannot be attributed

to LinMOKE or QMOKE, solely. For the quantitative description of our experimental data, we expand the Taylor series of the permittivity tensor up to third order in  $\mathbf{M}$ . We analyze the impact of structural domain twinning and the external magnetic field experimentally. We find that twinned Ni films provide a reduced threefold angular dependence of CMOKE. Thus, the observed MOKE contributions might be important for future applications related to structural domain twinning analysis, such as the investigation of huge magnetostriction in Ni<sub>2</sub>MnGa [37], or other so far non-identified features connected to CMOKE.

*II. Theoretic description* - MOKE can be related to the permittivity of the optically active, ferromagnetic layer. Hence, the Kerr angles  $\Phi_{s/p}$  for  $s$ - and  $p$ -polarized incident light write [38]

$$\Phi_s = \theta_s + i\epsilon_s = A_s \left( \epsilon_{yx} - \frac{\epsilon_{yz}\epsilon_{zx}}{\epsilon_d} \right) + B_s \epsilon_{zx} , \quad (1)$$

$$\Phi_p = \theta_p + i\epsilon_p = -A_p \left( \epsilon_{xy} - \frac{\epsilon_{xz}\epsilon_{zy}}{\epsilon_d} \right) + B_p \epsilon_{xz} , \quad (2)$$

in which  $\theta_{s/p}$  is the Kerr rotation and  $\epsilon_{s/p}$  is the Kerr ellipticity.  $A_{s/p}$  and  $B_{s/p}$  are the optical weighting factors which are even and odd functions of the angle of incidence, respectively.  $\epsilon_d$  represents the non-magnetic diagonal permittivity tensor elements of a cubic crystal structure.

In order to describe QMOKE, the permittivity tensor  $\epsilon$  is typically developed up to second order in  $\mathbf{M}$  [13, 25, 39]. However, to successfully describe all experimental observations presented in our study, we have to develop  $\epsilon$  up to third order in  $\mathbf{M}$ . Using the Einstein summation, the elements of  $\epsilon$  are expressed as

$$\varepsilon_{ij} = \varepsilon_{ij}^{(0)} + K_{ijk}M_k + G_{ijkl}M_kM_l + H_{ijklm}M_kM_lM_m. \quad (3)$$

Here,  $\varepsilon_{ij}^{(0)}$  describes the elements of the non-perturbed permittivity tensor.  $M_{k/l/m}$  are components of the normalized magnetization  $\mathbf{M}$ , and  $K_{ijk}$  and  $G_{ijkl}$  are the components of the linear and quadratic magneto-optic (MO) tensors  $\mathbf{K}$  and  $\mathbf{G}$  [40], respectively. We further add the components  $H_{ijklm}$  of the cubic MO five-rank tensor  $\mathbf{H}$  [33].

Using the Onsager relation  $\varepsilon_{ij}(\mathbf{M}) = \varepsilon_{ij}(-\mathbf{M})$  as well as symmetry arguments of cubic crystal structures, these tensors can be simplified in such a way that  $\mathbf{K}$  is solely determined by one independent parameter  $K$ , while  $\mathbf{G}$  is described by two independent parameters, namely  $G_s = (G_{11} - G_{12})$  and  $2G_{44}$  [28, 39]. The difference of these two parameters  $\Delta G = G_s - 2G_{44}$  denotes the anisotropic strength of  $\mathbf{G}$  [13, 21].  $\mathbf{H}$  possesses two independent parameters [32] which can be named  $H_{123}$  and  $H_{125}$  following the derivation in Ref. [32]. Moreover, we introduce an anisotropy parameter  $\Delta H = H_{123} - 3H_{125}$  which describes the anisotropic strength of  $\mathbf{H}$ .

In order to yield the perturbed permittivity tensor for a (111)-oriented cubic crystal structure, the permittivity tensor is transformed from (001) orientation to (111) orientation (see Supplemental Materials [41]). To describe the in-plane sample rotation in our experiment, we further apply a rotation to the permittivity tensor by the general angle  $\alpha$  around the out-of-plane [111] direction. The respective expressions for the permittivity tensor elements are written down in the Supplemental Materials [41].

*III. Eight-directional method* - In order to analyze individual MOKE contributions with different dependencies on  $\mathbf{M}$  experimentally, a separation algorithm, known as the eight-directional-method [42], can be used. So far, this method or similar ones have been utilized to characterize (001)- and (011)-oriented thin films of cubic crystal structure [28, 43] while the QMOKE in (111)-oriented thin films so far has been identified only by magnetization loop symmetrization [44] and theoretically [45]. During the eight-directional method, the MOKE signal is measured for eight different in-plane magnetization directions  $\mu = 0^\circ + k \cdot 45^\circ, k = \{0, 1, \dots, 7\}$  (see Supp. Mat. [41]). From these measurements, four different MOKE contributions are extracted. Analytical equations for each of the four MOKE contributions can be derived by inserting the permittivity tensor elements into the Eqs. (1) and (2). Note that we only consider contributions up to third order in  $\mathbf{M}$  and stick to in-plane magnetization. The first MOKE contribution separated by the eight-directional method is the LMOKE contribution including

CMOKE given by

$$\begin{aligned} \Phi_{M_L, M_L^3} &= \frac{1}{2} \left( \Phi_{s/p}^{\mu=90^\circ} - \Phi_{s/p}^{\mu=270^\circ} \right) \\ &= \pm B_{s/p} \left( K + \frac{H_{123} + 3H_{125}}{2} \right) \\ &\quad - A_{s/p} \frac{\sqrt{2}}{6} \left( \Delta H + \frac{K\Delta G}{\varepsilon_d} \right) \sin(3\alpha). \end{aligned} \quad (4)$$

Here, we can identify an isotropic term  $\propto M_L$  and  $\propto M_L^3$  as well as an anisotropic threefold term  $\propto M_L^3$ . The longitudinal component  $M_L$  describes the in-plane magnetization parallel to the plane of incidence. The amplitude of the anisotropic contribution is stemming from two MO parameters, being  $\Delta H$  and the product  $K\Delta G$ . The latter stems from the intermixing of  $\varepsilon_{yz}\varepsilon_{zx}$  and  $\varepsilon_{xz}\varepsilon_{zy}$  in Eqs. (1) and (2).

The second MOKE contribution is the CMOKE contribution of the transverse magnetization component

$$\begin{aligned} \Phi_{M_T^3} &= \frac{1}{2} \left( \Phi_{s/p}^{\mu=0^\circ} - \Phi_{s/p}^{\mu=180^\circ} \right) \\ &= A_{s/p} \frac{\sqrt{2}}{6} \left( \Delta H + \frac{K\Delta G}{\varepsilon_d} \right) \cos(3\alpha) \end{aligned} \quad (5)$$

which only consists of an anisotropic threefold term  $\propto M_T^3$ , with  $M_T$  being the in-plane magnetization perpendicular to the plane of incidence. In contrast to  $\Phi_{M_L, M_L^3}$ ,  $\Phi_{M_T^3}$  depends on  $\cos(3\alpha)$  instead of  $\sin(3\alpha)$ , but has the same amplitude.

The third MOKE contribution is the QMOKE contribution

$$\begin{aligned} \Phi_{M_L M_T} &= \frac{1}{2} \left( \Phi_{s/p}^{\mu=45^\circ} + \Phi_{s/p}^{\mu=225^\circ} - \Phi_{s/p}^{\mu=135^\circ} - \Phi_{s/p}^{\mu=315^\circ} \right) \\ &= \pm A_{s/p} \left( 2G_{44} + \frac{1}{3}\Delta G - \frac{K^2}{\varepsilon_d} \right) \\ &\quad - B_{s/p} \frac{\sqrt{2}}{3} \Delta G \sin(3\alpha) \end{aligned} \quad (6)$$

which is proportional to  $M_L M_T$ . It consists of an anisotropic threefold term and an isotropic term that depends on the MO parameters of  $\mathbf{G}$  as well as  $K^2$ .

The fourth and final MOKE contribution determined by the eight-directional method is the QMOKE contribution

$$\begin{aligned} \Phi_{M_T^2 - M_L^2} &= \frac{1}{2} \left( \Phi_{s/p}^{\mu=0^\circ} + \Phi_{s/p}^{\mu=180^\circ} - \Phi_{s/p}^{\mu=90^\circ} - \Phi_{s/p}^{\mu=270^\circ} \right) \\ &= -B_{s/p} \frac{\sqrt{2}}{3} \Delta G \cos(3\alpha) \end{aligned} \quad (7)$$

which is proportional to  $M_T^2 - M_L^2$  and only consists of an anisotropic threefold term. While  $\Phi_{M_T^2 - M_L^2}$  depends on  $\cos(3\alpha)$ , the anisotropic part of  $\Phi_{M_L M_T}$  depends on  $\sin(3\alpha)$ , but with the same amplitude including  $\Delta G$ .

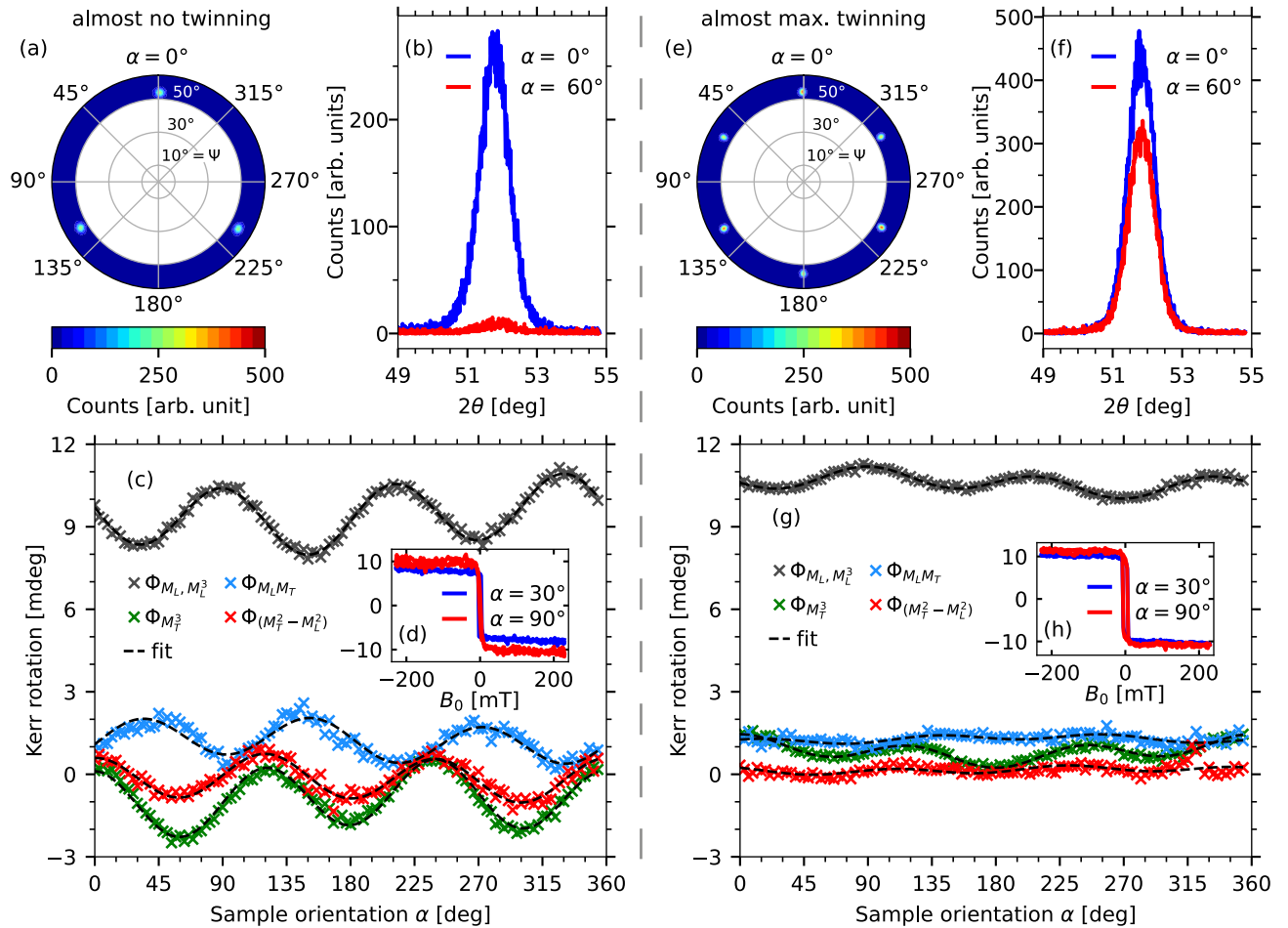


FIG. 1. XRD and MOKE data of the Ni(111) samples with almost no twinning (left) and almost maximum twinning (right). (a,e) Off-specular XRD scan (Euler's cradle texture map) showing the Ni{200} peaks at  $2\theta = 51.832^\circ$ . (b,f) XRD  $\theta - 2\theta$  scans of the Ni{200} peaks at selected  $\alpha$  angles. (c,g) Eight-directional method performed with a magnetic field strength of 230 mT using a wavelength of 635 nm. The dependence of four MOKE contributions on the sample orientation  $\alpha$  is demonstrated. (d,h) Magnetization curves for exemplary sample orientations.

*IV. Experimental background* - Two fcc Ni(111) thin films were prepared by magnetron sputtering onto MgO(111) substrates in an Ar atmosphere of  $2.1 \times 10^{-3}$  mbar. Parts of the growth procedure have been adapted from Ref. [46]. The substrate of sample 1 has been ultrasonically cleaned in acetone, isopropanol and ethanol for 15 minutes each and then dried in  $N_2$ . Both substrates were then annealed in vacuum at  $800^\circ\text{C}$ . The substrate of sample 1 was annealed for 1h, the one of sample 2 for 15 minutes. About 20 nm thick Ni layers were then deposited onto the substrates with a growth rate of 0.066 nm/s at a substrate temperature of  $350^\circ\text{C}$ . Afterwards, the Ni layers were capped with approximately 3 nm of Si which was grown at room temperature. The Ni layer thicknesses were confirmed by X-ray reflectivity measurements (see Supp. Mat. [41]), using the Cu  $K_\alpha$  source of a Phillips X'pert Pro MPD PW3040-60 diffractometer. Specular X-ray diffraction (XRD)  $\theta-2\theta$  scans (see Supp. Mat. [41]) as well as off-specular XRD texture mapping using an Euler cradle were employed

to examine the crystalline growth of the samples. The texture measurements were performed for  $360^\circ$  of sample rotation  $\alpha$  with a tilt of the samples  $\Psi = \langle 50^\circ, 60^\circ \rangle$ , effectively capturing the Ni{200} diffraction peaks. Since the Ni layer is grown in a (111) orientation, there are two growth types possible (structural domain twinning) which differ from each other by an in-plane rotation of  $60^\circ$ . Each (111) phase produces a diffraction pattern with threefold symmetry, but with a  $\Delta\alpha = 60^\circ$  difference between the patterns.

MOKE measurements were carried out using s-polarized light of 406 nm and 635 nm wavelengths and a  $45^\circ$  angle of incidence. Both the samples as well as the magnetic field were rotated in the sample plane. More detailed descriptions of the MOKE setup can be found in Refs. [47, 48].

*V. Results* - The off-specular XRD texture mapping of sample 1 is presented in Fig. 1(a). The scan was performed at  $2\theta=51.832^\circ$  and thus shows the Ni{200}

peaks. Additional  $\theta$ - $2\theta$  scans at all Ni{200} peak positions were made and are displayed exemplarily in Fig. 1(b). The appearance of only three intense Ni{200} peaks indicates that almost no twinning occurs in sample 1. The integrated peak intensities of the dominant phase make up 95.1% of the combined peak intensities.

The in-plane angular dependencies of the four MOKE contributions are measured by the eight-directional method according to Eqs. (4)-(7) and presented in Fig. 1(c). The experimentally observed dependencies are in good agreement with the analytical equations. In all four MOKE contributions, pronounced threefold angular dependencies are visible. While  $\Phi_{M_L, M_L^3}$  and  $\Phi_{M_L M_T}$  follow a  $\sin(3\alpha)$  curve (see Eqs. (4) and (6)),  $\Phi_{M_T^3}$  and  $\Phi_{M_T^2 - M_L^2}$  describe a  $\cos(3\alpha)$  behaviour (see Eqs. (5) and (7)). In addition, the expected offsets of  $\Phi_{M_L, M_L^3}$  and  $\Phi_{M_L M_T}$  can be identified (see Eqs. (4) and (6)), while  $\Phi_{M_T^2 - M_L^2}$  has a vanishing offset (see Eq. (7)).  $\Phi_{M_T^3}$  shows a finite offset which is not predicted by theory (see Eq. (5)). Setup misalignments as a possible origin of this offset have been excluded (see Supp. Mat. [41]). A small superimposed onefold angular dependence can be seen mainly in the  $\Phi_{M_L, M_L^3}$  and  $\Phi_{M_T^3}$  contributions. We attribute it to a vicinal MOKE (VISMOKE) contribution [38] caused by a slight miscut of the Ni layer (see Supp. Mat. [41] for further details). The off-specular XRD texture mapping and  $\theta$ - $2\theta$  scans of the Ni{200} peaks of sample 2 are displayed in Figs. 1(e,f). Here, six peaks of similar intensity can be identified. The dominant phase makes up 57.0% of the combined peak intensities. In all four MOKE contributions displayed in Fig. 1(g), the threefold angular dependencies have undergone a clear reduction, compared to sample 1. Exemplary magnetization curves at  $\alpha = 30^\circ, 90^\circ$  are displayed for both samples in Figs. 1(d) and 1(h), respectively. A stronger anisotropy in the saturation values can be identified in sample 1 compared to sample 2 due to the lower degree of twinning.

In order to analyze offsets, amplitudes and phase dependencies quantitatively, fits of the form  $C + A_1 \sin(3\alpha + \alpha_1) + A_2 \sin(\alpha + \alpha_2)$  have been performed (see dashed lines in Figs. 1(c) and 1(g)). Here, the onefold sine contribution is related to VISMOKE and the phase shift  $\alpha_2$  correlates with the miscut direction of the respective Ni film (see Supp. Mat. [41]). The phase shifts  $\alpha_1$  of all eight contributions are in good agreement to each other with additional  $90^\circ$  offset for  $\alpha_1$  of  $\Phi_{M_T^3}$  and  $\Phi_{M_T^2 - M_L^2}$  due to the  $\cos(3\alpha)$  dependence instead of  $\sin(3\alpha)$  (see Eqs. (4)-(7)). As predicted by theory, both CMOKE contributions  $\Phi_{M_L, M_L^3}$  and  $\Phi_{M_T^3}$  have similar absolute amplitudes of the threefold angular dependencies. For sample 1, these are  $(1.17 \pm 0.01)$  mdeg and  $(1.16 \pm 0.02)$  mdeg. In sample 2, both of these amplitudes are reduced to  $(0.33 \pm 0.01)$  mdeg. The

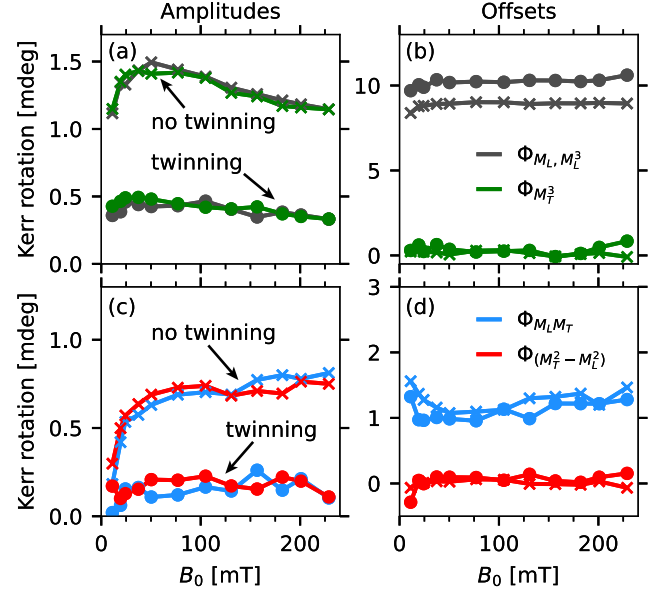


FIG. 2. Dependence of individual MOKE contributions on the applied magnetic field for a wavelength of 635 nm. Shown are (a,c) absolute amplitudes and (b,d) offsets for the samples with (dotted data points) and almost no twinning (crosses).

QMOKE contributions  $\Phi_{M_L M_T}$  and  $\Phi_{M_T^2 - M_L^2}$  also show similar amplitudes for each sample. In sample 1, these are  $(0.71 \pm 0.03)$  mdeg and  $(0.77 \pm 0.02)$  mdeg. In sample 2, these amplitudes are reduced to  $(0.10 \pm 0.01)$  mdeg and  $(0.11 \pm 0.02)$  mdeg. The reduction of the QMOKE contributions is slightly stronger than the reduction of the CMOKE contributions.

The offsets of  $\Phi_{M_L, M_L^3}$  and  $\Phi_{M_L M_T}$  in samples 1 and 2 are mainly independent from the degree of twinning. Slight variations between the offsets can be attributed to minor variations in layer thicknesses. Measurements of the Kerr ellipticity and with  $\lambda = 406$  nm have also been conducted using the eight-directional method (see Supp. Mat. [41]). The same reduction of CMOKE and QMOKE amplitudes with the degree of twinning has been observed, while the offsets stay constant.

The dependencies of the amplitudes and offsets on the magnetic field strength are displayed in Fig. 2.  $\Phi_{M_L, M_L^3}$  and  $\Phi_{M_T^3}$  have similar amplitudes, just as  $\Phi_{M_L M_T}$  and  $\Phi_{M_T^2 - M_L^2}$ , which is also predicted by Eqs. (4)-(7). Again, the amplitudes of all MOKE contributions (Figs. 2(a,c)) are smaller for the twinned sample compared to the sample with almost no twinning, while the offsets of all MOKE contributions (Figs. 2(b,d)) are independent from twinning. Only the offset of  $\Phi_{M_L, M_L^3}$  deviates slightly (black data in Fig. 2(b)) due to small differences in the Ni thicknesses. The first data points of the magnetic field dependence up to a few tens of mT belong to the magnetically unsaturated Ni layer. Here, the data deviates from the residual data progress at larger magnetic field strengths. However, when the samples are magnetically saturated, a



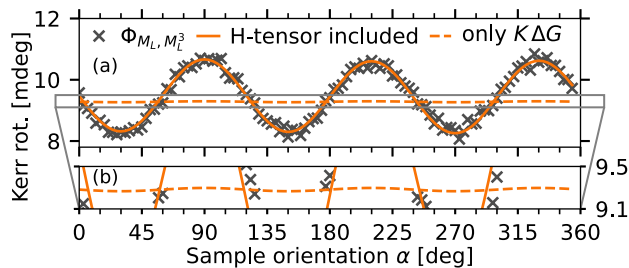


FIG. 3.  $\Phi_{M_L, M_L^3}$  contribution without VISMOKE. (a) Simulations with and without the permittivity tensor of third order in  $\mathbf{M}$  are shown. (b) Close-up of the simulation without the  $\mathbf{H}$  tensor.

decrease of the CMOKE amplitudes with increasing magnetic field (Fig. 2(a)) and a slight increase of the QMOKE amplitudes of the non-twinned sample (Fig. 2(c)) still remain. Most offsets do not show a dependence on the magnetic field strength if the Ni layer is saturated (Fig. 2(b,d)). Only the  $\Phi_{M_L M_T}$  offset increases slightly with increasing magnetic field strength.

*VI. Numerical simulations* - The CMOKE threefold angular dependence can be described qualitatively just by  $K \Delta G$  (see Eqs. (4) and (5)). In order to check whether the  $\mathbf{H}$  tensor is needed to quantitatively describe the amplitude of the CMOKE oscillations, numerical simulations using Yeh's transfer matrix formalism [49] with and without the tensor  $\mathbf{H}$  have been conducted. In the numerical model, the MO parameters are set as free parameters and the model is fitted to the experimental data.

In Fig. 3(a), simulations with and without  $\mathbf{H}$  tensor are shown for sample 1. Although the fit was performed for all contributions of the eight-directional method simultaneously, we only show the results for  $\Phi_{M_L, M_L^3}$  here (see Supp. Mat. [41] for the numerical simulation of all MOKE contributions). The superimposed onefold angular dependency due to VISMOKE has been subtracted prior to the numerical fitting. The simulation of MOKE up to second order in  $\mathbf{M}$  (i.e. without  $\mathbf{H}$ ) shows negligible angular dependencies of  $\Phi_{M_L, M_L^3}$  (see Fig. 3(b)). In order to describe  $\Phi_{M_L, M_L^3}$  solely by  $K$  and  $\Delta G$  in the numerical model, the calculated amplitudes for  $\Phi_{M_L M_T}$  and  $\Phi_{M_T^2 - M_L^2}$  would be largely above the experimental values. However, with the  $\mathbf{H}$  tensor included in the simulation, CMOKE and the QMOKE contributions can be fitted well, simultaneously. Therefore, the contribution which is stemming from  $K \Delta G$  can be assumed to be small compared to the contribution stemming from  $\Delta H$ . This shows that the  $\mathbf{H}$  tensor is indispensable for a quantitative description of CMOKE in Ni(111) films.

*VII. Conclusion* - We observed MOKE contributions of third order in  $\mathbf{M}$ , called CMOKE, in Ni(111) thin films.

These contributions manifest themselves in strong threefold angular dependencies of e.g. LMOKE which are even larger than the ones of the QMOKE contributions. We were able to describe CMOKE quantitatively by describing the permittivity tensor up to third order in  $\mathbf{M}$  and including the fifth-rank tensor  $\mathbf{H}$ . Furthermore, we showed that the angular dependencies of the different MOKE contributions are suppressed in case of structural domain twinning. Finally, the slight magnetic field dependence of CMOKE and QMOKE in the saturated samples will be investigated in future experiments using much larger magnetic fields. Our findings can be used in new applications of vectorial magnetometry, spectroscopy and microscopy in connection with structural domain twinning analysis.

### ACKNOWLEDGMENTS

J.H. acknowledges support by the Czech Science Foundation (GACR), Grant No. GA19-13310S, and by the European Union project Matfun, Project No. CZ.02.1.01/0.0/0.0/15\_003/0000487. R.S. acknowledges support by the European Regional Development Fund, Project No. CZ. 02.1.01/0.0/0.0/16\_013/0001791.

\* contributed to this work equally  
 † tkuschel@physik.uni-bielefeld.de

- [1] J. Kerr, *The London, Edinburgh, and Dublin Philosophical Magazine and Journal of Science* **3**, 321 (1877).
- [2] E. R. Moog and S. D. Bader, *Superlattices and Microstructures* **1**, 543 (1985).
- [3] Z. Q. Qiu and S. D. Bader, *Review of Scientific Instruments* **71**, 1243 (2000).
- [4] J. M. Florczak and E. D. Dahlberg, *Journal of Applied Physics* **67**, 7520 (1990).
- [5] P. Vavassori, *Applied Physics Letters* **77**, 1605 (2000).
- [6] G. R. Harp, D. Weller, T. A. Rabedeau, R. F. C. Farrow, and M. F. Toney, *Physical Review Letters* **71**, 2493 (1993).
- [7] M. Veis, L. Beran, R. Antos, D. Legut, J. Hamrle, J. Pistora, C. Sterwerf, M. Meinert, J.-M. Schmalhorst, T. Kuschel, and G. Reiss, *Journal of Applied Physics* **115**, 17A927 (2014).
- [8] R. Schäfer, ed., *Investigation of domains and dynamics of domain walls by the magneto-optical Kerr-effect*, Handbook of Magnetism and Advanced Magnetic Materials (John Wiley & Sons, Ltd., 2007).
- [9] J. McCord, *Journal of Physics D: Applied Physics* **48**, 333001 (2015).
- [10] E. Beaupaire, J.-C. Merle, A. Daunois, and J.-Y. Bigot, *Physical Review Letters* **76**, 4250 (1996).
- [11] A. Kirilyuk, A. V. Kimel, and T. Rasing, *Reviews of Modern Physics* **82**, 2731 (2010).
- [12] G. Metzger, P. Pluvinaige, and R. Torguet, *Annale de Physique* **13**, 5 (1965).
- [13] J. Hamrle, S. Blomeier, O. Gaier, B. Hillebrands, H. Schneider, G. Jakob, K. Postava, and C. Felser, *Journal of Physics D: Applied Physics* **40**, 1563 (2007).

- [14] V. Saidl, P. Němec, P. Wadley, V. Hills, R. P. Campion, V. Novák, K. W. Edmonds, F. Maccherozzi, S. S. Dhesi, B. L. Gallagher, F. Trojánek, J. Kuneš, J. Železný, P. Malý, and T. Jungwirth, *Nature Photonics* **11**, 91 (2017).
- [15] Z. Zheng, J. Y. Shi, Q. Li, T. Gu, H. Xia, L. Q. Shen, F. Jin, H. C. Yuan, Y. Z. Wu, L. Y. Chen, and H. B. Zhao, *Phys. Rev. B* **98**, 134409 (2018).
- [16] H. C. Zhao, H. Xia, S. Hu, Y. Y. Lv, Z. R. Zhao, J. He, E. Liang, G. Ni, L. Y. Chen, X. P. Qiu, S. M. Zhou, and H. B. Zhao, *Nature Communications* **12**, 5266 (2021).
- [17] G. Wolf, J. Hamrle, S. Trudel, T. Kubota, Y. Ando, and B. Hillebrands, *Journal of Applied Physics* **110**, 043904 (2011).
- [18] R. Silber, D. Král, O. Stejskal, T. Kubota, Y. Ando, J. Pištora, M. Veis, J. Hamrle, and T. Kuschel, *Applied Physics Letters* **116**, 262401 (2020).
- [19] M. Montazeri, P. Upadhyaya, M. C. Onbasli, G. Yu, K. L. Wong, M. Lang, Y. Fan, X. Li, P. Khalili Amiri, R. N. Schwartz, C. A. Ross, and K. L. Wang, *Nature Communications* **6**, 8958 (2015).
- [20] T. Mewes, H. Nembach, M. Rickart, and B. Hillebrands, *Journal of Applied Physics* **95**, 5324 (2004).
- [21] T. Kuschel, H. Bardenhagen, H. Wilkens, R. Schubert, J. Hamrle, J. Pištora, and J. Wollschläger, *Journal of Physics D: Applied Physics* **44**, 265003 (2011).
- [22] N. Tesařová, P. Němec, E. Rozkotová, J. Šubrt, H. Reichlová, D. Butkovičová, F. Trojánek, P. Malý, V. Novák, and T. Jungwirth, *Applied Physics Letters* **100**, 102403 (2012).
- [23] N. Tesařová, P. Němec, E. Rozkotová, J. Zemen, T. Janda, D. Butkovičová, F. Trojánek, K. Olejník, V. Novák, P. Malý, and T. Jungwirth, *Nature Photonics* **7**, 492 (2013).
- [24] H. Jang, L. Marnitz, T. Huebner, J. Kimling, T. Kuschel, and D. G. Cahill, *Phys. Rev. Applied* **13**, 024007 (2020).
- [25] B. Sepúlveda, Y. Huttel, C. Martínez Boubeta, A. Ce Bollada, and G. Armelles, *Physical Review B* **68**, 064401 (2003).
- [26] J. Hamrlová, D. Legut, M. Veis, J. Pištora, and J. Hamrle, *Journal of Magnetism and Magnetic Materials* **420**, 143 (2016).
- [27] R. Silber, M. Tomíčková, J. Rodewald, J. Wollschläger, J. Pištora, M. Veis, T. Kuschel, and J. Hamrle, *Photonics and Nanostructures - Fundamentals and Applications* **31**, 60 (2018).
- [28] R. Silber, O. Stejskal, L. Beran, P. Cejpek, R. Antos, T. Matalla-Wagner, J. Thien, O. Kuschel, J. Wollschläger, M. Veis, T. Kuschel, and J. Hamrle, *Physical Review B* **100**, 064403 (2019).
- [29] T. Janda, L. Nádvořník, J. Kuchařík, D. Butkovičová, E. Schmoranzarová, F. Trojánek, and P. Němec, *Review of Scientific Instruments* **89**, 073703 (2018).
- [30] J. Xu, C. Zhou, M. Jia, D. Shi, C. Liu, H. Chen, G. Chen, G. Zhang, Y. Liang, J. Li, W. Zhang, and Y. Wu, *Phys. Rev. B* **100**, 134413 (2019).
- [31] V. N. Gridnev, B. B. Krichevstov, V. V. Pavlov, and R. V. Pisarev, *Journal of Experimental and Theoretical Physics Letters* **65**, 68 (1997).
- [32] A. V. Petukhov, T. Rasing, T. Katayama, N. Nakajima, and Y. Suzuki, *Journal of Applied Physics* **83**, 6742 (1998).
- [33] K. Postava, J. Pištora, and T. Yamaguchi, *Sensors and Actuators A: Physical* **110**, 242 (2004).
- [34] W. Limmer, M. Glunk, J. Daeubler, T. Hummel, W. Schoch, R. Sauer, C. Bihler, H. Huebl, M. S. Brandt, and S. T. B. Goennenwein, *Phys. Rev. B* **74**, 205205 (2006).
- [35] W. Limmer, J. Daeubler, L. Dreher, M. Glunk, W. Schoch, S. Schwaiger, and R. Sauer, *Phys. Rev. B* **77**, 205210 (2008).
- [36] S. Meyer, R. Schlitz, S. Geprägs, M. Opel, H. Huebl, R. Gross, and S. T. B. Goennenwein, *Applied Physics Letters* **106**, 132402 (2015).
- [37] D. Musienko, F. Nilsén, A. Armstrong, M. Rameš, P. Verčát, R. H. Colman, J. Čapek, P. Müllner, O. Heczko, and L. Straka, *Journal of Materials Research and Technology* **14**, 1934 (2021).
- [38] J. Hamrle, J. Ferré, J. P. Jamet, V. Repain, G. Baudot, and S. Rousset, *Physical Review B* **67**, 155411 (2003).
- [39] Š. Višňovský, *Optics in Magnetic Multilayers and Nanostructures* (CRC Press, Boca Raton, 2006).
- [40] Š. Višňovský, *Czechoslovak Journal of Physics* **36**, 1424 (1986).
- [41] See Supplemental Materials at [URL will be inserted by publisher] including Refs. [50–52].
- [42] K. Postava, D. Hrabovský, J. Pištora, A. R. Fert, Š. Višňovský, and T. Yamaguchi, *Journal of Applied Physics* **91**, 7293 (2002).
- [43] J. H. Liang, Y. L. Chen, L. Sun, C. Zhou, Y. Yang, and Y. Z. Wu, *Applied Physics Letters* **108**, 082404 (2016).
- [44] P. K. Muduli, W. C. Rice, L. He, B. A. Collins, Y. S. Chu, and F. Tsui, *Journal of Physics: Condensed Matter* **21**, 296005 (2009).
- [45] J. Hamrlová, J. Hamrle, K. Postava, and J. Pištora, *physica status solidi (b)* **250**, 2194 (2013).
- [46] P. Sandström, E. B. Svedberg, J. Birch, and J.-E. Sundgren, *Surface Science* **437**, L767 (1999).
- [47] A. Kehlberger, K. Richter, M. C. Onbasli, G. Jakob, D. H. Kim, T. Goto, C. A. Ross, G. Götz, G. Reiss, T. Kuschel, and M. Kläui, *Physical Review Applied* **4**, 014008 (2015).
- [48] N. D. Müglich, A. Gaul, M. Meyl, A. Ehresmann, G. Götz, G. Reiss, and T. Kuschel, *Physical Review B* **94**, 184407 (2016).
- [49] P. Yeh, *Surface Science* **96**, 41 (1980).
- [50] L. G. Parratt, *Physical Review* **95**, 359 (1954).
- [51] M. Björck and G. Andersson, *Journal of Applied Crystallography* **40**, 1174 (2007).
- [52] G. Mende, J. Finster, D. Flamm, and D. Schulze, *Surface Science* **128**, 169 (1983).